Solar Energy 301 (2025) 113865

Contents lists available at ScienceDirect

Solar Energy

journal homepage: www.elsevier.com/locate/solener

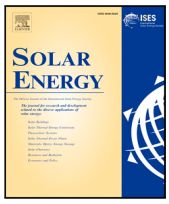

A fully convolutional neural network to interpolate solar irradiation NWP ensemble forecasts

Matthias Zech *, Annette Hammer, Lueder von Bremen

German Aerospace Center (DLR), Institute of Networked Energy Systems, Carl-von-Ossietzky-Str. 15, Oldenburg, 26129, Germany

ARTICLE INFO

MSC:
62M45

Keywords:
Energy meteorology
Temporal interpolation
Deep learning
Machine learning
Probabilistic forecasting

ABSTRACT

NWP ensemble forecasts have proven to be a reliable resource for solar irradiation estimates for the next few hours up to multiple days ahead. Due to the substantial storage requirements for saving NWP ensemble outputs, ensemble forecasts often have limited spatio-temporal resolutions. However, decision-making under uncertainty based on these ensemble forecasts typically requires more detailed temporal information. To fill this gap, this paper introduces a method based on fully convolutional neural networks (U-Net) to interpolate missing time steps for both deterministic and probabilistic solar irradiation forecasts. The model is trained on deterministic forecasts (ECMWF IFS) to restore hourly forecasts from three-hourly forecasts benefiting from past physical NWP model runs. We show that the proposed method is capable of restoring deterministic forecasts and furthermore can provide highly accurate probabilistic solar irradiation forecast interpolations, as verified on reanalysis and satellite data. The method only requires extraterrestrial irradiation as auxiliary input instead of clear-sky irradiation, making the proposed method a versatile and performant tool for interpolating solar irradiation forecasts for both cloudless and cloudy conditions.

1. Introduction

Accurate solar irradiation forecasts can increase the integration of solar energy into electrical power grids and reduce the associated integration cost [1]. Solar energy research and industry have largely focused on deterministic forecasts, which provide only point estimates, neglecting the large natural uncertainty of solar irradiation forecasts, in particular with increasing lead times. More recently, probabilistic forecasts gained more interest as they are able to provide in addition to a point forecast a corresponding uncertainty [1]. This uncertainty information is valuable when used within decision support tools such as optimization under uncertainty models [2], to derive the optimal bidding behavior of power plant portfolios in sequential electricity markets [3], or to determine the economic dispatch under techno-economic constraints [4]. As energy is traded in sequential energy markets with different gate closing times [5], sequential decisions are also made at different stages requiring forecasts with different lead times. With most decisions taken in day-ahead energy markets, accurate day-ahead solar irradiation forecasts are needed at which dynamical numerical weather prediction (NWP) models excel [6–8] and continually improve [9].

NWP models describe the evolution of the atmospheric system based on the description of the initial conditions, derived from tremendous data assimilation, and its evolution through physical laws. Ensemble forecasts have evolved as a reliable tool for estimating forecast uncertainties by running dynamical model runs with different initial conditions, parameter values, and stochastic forcings, which creates a set of independent and physically consistent realizations of future weather [10–12]. In solar energy forecasting, NWP ensemble forecasts have been used to provide estimates of solar energy uncertainty [13, 14]. However, NWP ensembles are usually provided in limited spatio-temporal resolution while decision-making, such as trading decisions, ever seek for shorter time scales to derive more precise decisions.

The mismatch in temporal resolution between ensemble forecasts and decision-making can be resolved using temporal interpolation. However, examples in the solar research literature often rely on linear interpolation [15–17] through linear weightings of known time steps, which assumes a linear behavior of the atmosphere between two time steps. Although Lorenz et al. [15] shows that the impact of interpolation errors due to the diurnal cycle of solar irradiation can be effectively removed by normalizing through clear-sky irradiation, the main drawback of linear interpolation remains, namely assuming that the transition between two weather states is linear. To avoid interpolation biasses and allow non-linearities, we interpret the temporal interpolation as a supervised learning problem in which missing time steps are estimated through a parametric Machine Learning (ML)

* Corresponding author.
E-mail address: matthias.zech@dlr.de (M. Zech).

https://doi.org/10.1016/j.solener.2025.113865
Received 20 January 2025; Received in revised form 27 July 2025; Accepted 5 August 2025
Available online 15 September 2025

model which learns from past NWP model simulations. This approach seems highly promising given the large success of ML applications, and more specifically Deep Learning (DL), in weather forecasting. Within solar irradiation forecasting, DL has been applied to provide solar irradiance nowcasts based on satellite imagery [18,19]. Within NWP modeling, DL has shown promise for model parameterizations to represent non-resolved subgrid physical processes [20–23], for postprocessing [11,24–27] and more recently by proposing AI-driven weather models such as the GraphCast model [28], GenCast [29] or the ECMWF AIFS model [30], models that already run operationally providing deterministic and probabilistic forecasts and which show promising results [31].

Despite the prominent usage and success of ML within NWP and solar irradiation forecasting, applying DL to interpolate solar irradiation NWP model outputs has not yet been investigated, which is the aim of this study. Therefore, we train a DL-based model on deterministic forecasts and can show competitive performance for both deterministic and probabilistic forecast interpolations. Since the model only requires extraterrestrial irradiation as an auxiliary input, which can be efficiently computed using deterministic algorithms, the proposed method is not only effective, but also easy to apply across a wide range of applications. Furthermore, relying on fully convolutional neural networks allows the model to capture spatial information relevant for detailed cloud representation.

The organization of this paper is as follows. We begin with the methodology in Section 2, where we describe common interpolation methods, namely linear interpolation, scaled linear interpolation, and the proposed model. To better understand the importance of irradiation normalization, Section 3 compares the difference between interpolations based on the clearness and the clear-sky index and explains the resulting biasses from the clearness index based on a geometrical explanation. In the computational study in Section 4, we evaluate the ability to restore deterministic forecasts and the ability to interpolate missing time steps in the ECMWF EPS, a widely used ensemble forecasts. The results are summarized in Section 5, then discussed in Section 6 and finally concluded in Section 7.

2. Methodology

2.1. Reference methods

Before explaining the proposed architecture, we describe other common interpolation techniques that serve as a baseline for the proposed model. Note that we focus on irradiation maps I as the output of NWP models and that NWP models usually output accumulated solar energy over a time interval [Wh/m^2], which is referred to as solar irradiation in contrast to instantaneous solar irradiance [W/m^2].

2.1.1. Linear interpolation

Linear interpolation is a nonparametric method which calculates missing time steps based on the distance to the known forecasts. The interpolation is calculated based on the weighted average of the closest two known irradiation maps (I_1, I_2)

$$I_{\text{inter}} = w\, I_1 + \big(1-w\big) I_2, \qquad 0 < w < 1 \tag{1}$$

with weights w based on the distance to the known time steps. More illustratively, interpolating the 10-th hour of a day with known time steps at 09:00 and 12:00 can be calculated by

$$I_{10:00} = \frac{2}{3} I_{09:00} + \frac{1}{3} I_{12:00} \tag{2}$$

This method assumes a linear relationship between the transitions of weather situations which is inadequate for two reasons. First, the mathematical description of the evolution of weather as in NWP models does not follow linear equations but is usually described by a set of coupled non-linear partial differential equations based on the three major dynamic processes of advection, adjustment and diffusion as described in more detail in Riddaway [32]. Second, solar irradiation exhibits a strong diurnal cycle due to the apparent movement of the Sun, which results in varying magnitudes of solar radiation reaching the Earth's atmosphere. Since this movement follows a curved path, linear interpolation inevitably introduces a *diurnal cycle bias*.

2.1.2. Scaled linear interpolation

A simple yet effective way to avoid the diurnal cycle bias in linear interpolation is to normalize the irradiation by the maximum reachable irradiation $I' = \frac{I}{I^{max}}$. The scaled linear interpolation calculation is then identical to Eq. (2) but based on scaled irradiation (I') values

$$I'_{inter} = w I'_1 + (1-w) I'_2, \qquad 0 < w < 1 \tag{3}$$

Although mathematically simple, it is physically more difficult to determine the maximum irradiance quantity I^{max}. Linear interpolation and its normalized variant was first used in Lorenz et al. [15] and is a common technique in solar irradiance contexts [16]. Common values are extraterrestrial irradiation and clear-sky irradiation, which are compared in more detail in Section 3.

2.2. InterpNet

The proposed neural network implementation formulates the interpolation problem as a supervised learning problem in which the neural network aims to restore irradiation maps from a training history of past NWP model runs. For this case study, NWP runs with hourly resolution are used, with only every third hour retained as input. The intermediate hours are omitted and used as targets for training the model to restore the missing forecasts. The model architecture and the in- and outputs are shown in Fig. 1. The input comprises six different channels, which are two irradiation forecasts (I_0 and I_3) that specify the borders of the interpolation time window, the extraterrestrial irradiation of the two intermediate time steps (I_1^{ext}, I_2^{ext}), and the interpolated irradiation maps based on scaled linear interpolation using the clearness index (I_1^{IP}, I_2^{IP}) as described in Section 2.1.2. Integrating the interpolated images based on the clearness index simplifies the learning problem as the neural network already has a good guess of the output so that it can focus on polishing systematic interpolation errors.

The six input images are fed into a fully convolutional neural network based on the U-Net architecture from Ronneberger et al. [33] as visualized in Fig. 1 which is implemented in `pytorch` [34]. The U-Net architecture is a widely applied architecture for semantic segmentation in a broad range of applications and more specifically in solar energy research for instance for PV panel detection [35,36] and solar energy nowcasting [18]. The U-Net is characterized by an encoder and a symmetric decoder, which leads to its characteristic u-shape. The output images of the U-Net have the same resolution as the input images, which makes it appropriate for the problem of temporal interpolation. The output of the U-Net is continuous and has two channels for the respective interpolated images. The encoder of the U-Net describes the left part of the architecture which is characterized by decreasing image resolutions and an increasing number of which allows the U-Net to learn larger features at deeper stages within the encoder. Decreasing the image resolutions at the encoder stage is achieved through strided convolutions (stride size 2). The decoder part represents the counterpart of the encoder that is characterized by increasing image resolutions through upsampling and a decreasing number of filters of the convolutional layers. Furthermore, the U-Net architecture contains skip connections at the same depth between the encoder and decoder, as shown in Fig. 1, which allows fine-grained details to be recovered during learning. This feature is important not only for the initial application context of biomedical segmentation in Ronneberger et al. [33], but also in the context of this study to recover, for example, the spatial information of detailed cloud structures.

Neural network implementations can greatly benefit from reusing the weights of carefully designed and already trained architectures,

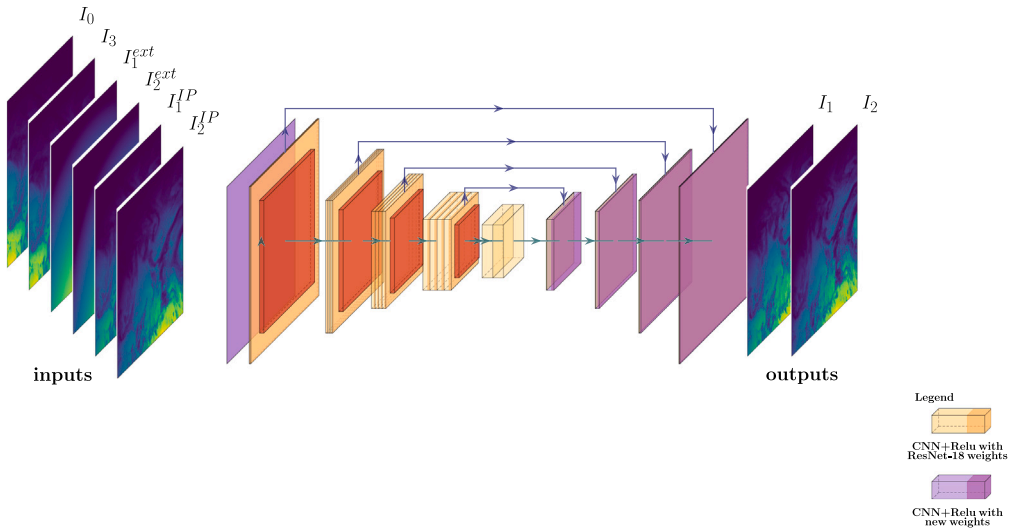

Fig. 1. InterpNet architecture. The purple arrows indicate skip connections, the green arrows the main forward direction through the U-Net architecture. The stacked input images represent the known aggregated solar irradiation values of the zeroth and the third hour (I_0, I_3), the extraterrestrial irradiation (I_1^{ext}, I_2^{ext}) and the interpolated irradiation values based on the clearness index (I_1', I_2') with the same hours as output images (I_1, I_2). More information about the U-Net characteristics can be found in Ronneberger et al. [33].

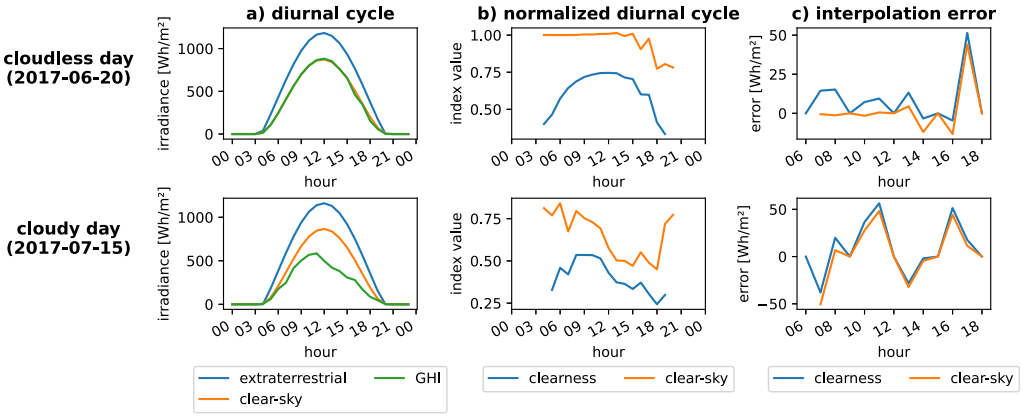

Fig. 2. Illustration of the diurnal cycle and interpolation errors based on reanalysis data (ERA5) during a cloudless and a cloudy day for a location in Northern Germany (50°N, 10°E). (a) shows the diurnal cycle of hourly global horizontal irradiance GHI, clear-sky and extraterrestrial irradiation. (b) shows clear-sky and clearness index for the same day. (c) shows the interpolation error when using the clearness or the clear-sky index.

which is more commonly known as transfer learning [37]. Therefore, the encoder of the U-Net architecture uses the ResNet-18 architecture [38] including its weights, which originate from neural networks trained on images from the ImageNet competition [39]. The ResNet architecture is based on three channels (RGB). To reduce the input images from six channels to three channels, convolutional layers with three kernels are stacked before the pretrained U-Net architecture to match the dimensions of the first layer of the encoder.

The model is trained using the Adam optimizer [40] based on an adaptable learning rate with a maximum learning rate derived from the range test as proposed in Smith and Topin [41]. It is trained on three years of training data (2013–2015) for 200 epochs with a batch size of 32 minimizing the mean squared error. The inputs are standardized for each channel separately and saved to be loaded for inference.

Note that the neural network only uses extraterrestrial irradiation instead of clear-sky irradiation as input. Because extraterrestrial irradiation is much easier to calculate than clear-sky irradiation, all auxiliary input needed for the InterpNet can be calculated without running an expensive radiative transfer model or without semi-empirical models.

3. The importance of correct normalization

This section discusses the usage of the clearness and the clear-sky indices for irradiance normalization. By this, the importance of proper normalization within interpolation is demonstrated. This helps towards a better understanding for the further course of this study.

3.1. Normalization by clearness or clear-sky index

A simple quantity for I^{max} is the *extraterrestrial irradiation* that refers to the solar energy that reaches the top of the atmosphere, ignoring the effect of the atmosphere. When used for normalization to obtain normalized solar irradiation map I', the resulting value is usually referred to as the *clearness index*. As extraterrestrial irradiation ignores the complex interaction between solar irradiation and the atmosphere, there are simple, computationally efficient deterministic algorithms based on solar geometry to calculate extraterrestrial irradiation such as described in [42].

A more accurate normalization can be achieved by considering atmospheric attenuation through the so-called *clear-sky irradiation*, or

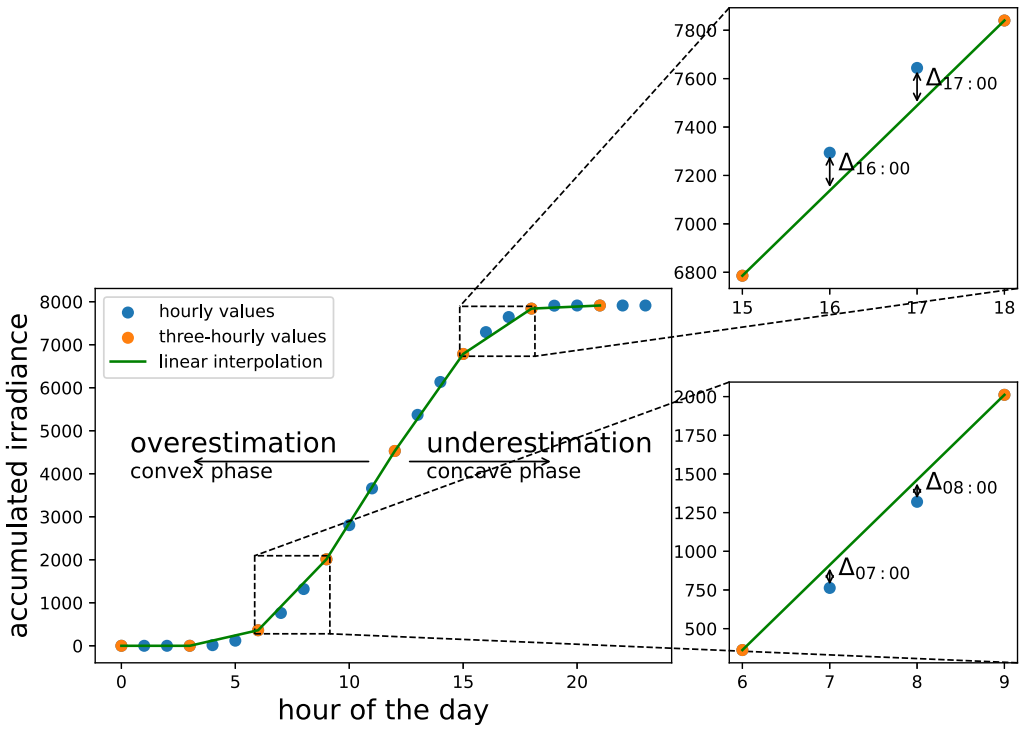

Fig. 3. Graphical illustration of the linear interpolation bias Δ_t for solar irradiation [Wh/m^2] on a cloudless day (2017-06-14, 50°N, 10°E).

Table 1
Qualitative derivation of the sign of the bias when using interpolation on aggregated solar irradiation. The underlined letter in the case definition represents the known forecast, meaning that (L̲R) represents an interpolation with known forecast on the left-hand side and no forecast known on the right-hand side. In the formulas, mathematical symbols in blue indicate interpolated values, the direction of the arrows indicates the bias with circle meaning no bias.

	Case 1 (L̲R)	Case 2 (LR)	Case 3 (LR̲)
Formula	$I_t = \hat{G}_t - G_{t-1}$	$I_t = \hat{G}_t - \hat{G}_{t-1}$	$I_t = G_t - \hat{G}_{t-1}$
Forenoon example	$I_{10:00} = \hat{G}_{10:00} - G_{09:00}$	$I_{11:00} = \hat{G}_{11:00} - \hat{G}_{10:00}$	$I_{12:00} = G_{12:00} - \hat{G}_{11:00}$
Forenoon bias	(↑) − (∘) = ↑	(↑) − (↑) = (∘)	(∘) − (↑) = (↓)
Afternoon bias	(↓) − (∘) = ↓	(↓) − (↓) = (∘)	(∘) − (↓) = (↑)

when normalized the *clear-sky index*, [43]. However, these require computationally expensive radiative transfer calculations or simplified parameterizations which both require additional meteorological input to derive atmospheric attenuation [44].

To better understand the effect of using clearness or clear-sky indices within interpolation, Fig. 2 shows the absolute extraterrestrial and clear-sky irradiation, the clearness and clear-sky indices, and the respective scaled interpolations on a cloudless day (2017-06-20) and a cloudy day (2017-07-15) in Northern Germany using ERA5 [45] data. Fig. 2a shows that extraterrestrial irradiation is constantly higher than clear-sky irradiation, as it ignores atmospheric attenuation. Furthermore, the clear-sky irradiation matches the GHI on the cloudless day, showing that the clear-sky model is well calibrated. When used for normalization, the clear-sky index shows low variability with values close to 1 except during the evening hours, while the clearness index shows poor normalization abilities. This leads to large errors when using for interpolation, as depicted in Fig. 2c. For the cloudy day (2017-07-15), these differences become minor due to the additional errors of the clouds.

3.2. Geometrical explanation of the diurnal cycle bias of linear interpolation

NWP irradiation forecasts refer to aggregates of irradiation over the forecast lead time. Thus, the 15:00 forecast represents the total irradiation reached until 15:00 whereas practical applications of solar energy require hourly values of irradiation (power) (14:00–15:00). To derive the amount of irradiation I from the aggregated forecasts G, the aggregates need to be subtracted

$$I_t = G_t - G_{t-1} \tag{4}$$

Due to the diurnal cycle, the integral of the clear-sky irradiation during one day has a characteristic S-curve as shown in Fig. 3. Linear temporal interpolation aims to fit linear curves between the known reference times (shown as orange dots). Simple mathematical considerations can aid in understanding the sign of the bias: The forenoon phase can be regarded as a convex function as it represents the integral of a strict monotonically increasing function until noon. Fitting a linear line between two arbitrary points of a convex function necessarily leads to an overestimation by the definition of convexity. The afternoon follows a concave function due to monotonically leading for linear interpolation to an underestimation. For illustration, Fig. 3 shows these two different situations for two zoomed-in time windows.

By knowing these resulting biasses, we can investigate the consequence for the case of interpolating solar irradiation aggregates as in this study. For this purpose, Table 1 shows the three cases of forecast interpolations, which means that we have a known integrated forecast on the left-hand side but only an interpolation of the right-hand side (L̲R), vice-versa (LR̲) or only interpolated forecasts (LR) with three different examples of the forenoon phase (10:00, 11:00, 12:00). At 10:00, we have one known aggregate (09:00) and one interpolated aggregate. As this interpolation originates from forenoon, we know it is overestimated leading to a positive bias for the 10:00 estimate. At

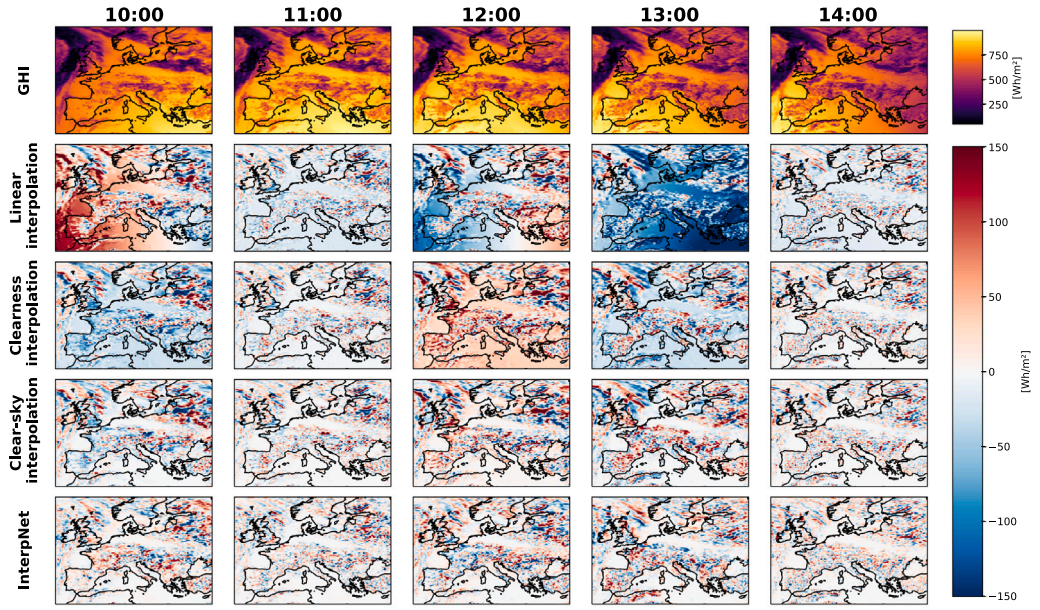

Fig. 4. Illustration of diurnal cycle bias of different interpolated solar irradiation maps (2017-06-01). The first row indicate the forecasted hourly solar irradiation and the rows below the forecast restoration error of the respective interpolation methods.

11:00, we have two interpolated values, both containing a positive bias leading to a smaller bias for subtraction. At 12:00, the interpolated value is subtracted from the known forecast, which leads to a negative bias. As all signs (except the known aggregates from the forecast) flip in the afternoon, the bias of the afternoon hours can be derived by inverting all signs as shown in Table 1.

4. Study design

4.1. Data and experiments

To evaluate InterpNet's performance, we designed a case study for both deterministic and probabilistic forecasts. The deterministic forecasts are verified on the omitted forecasts to evaluate the ability to restore forecasts (ECMWF IFS), while the probabilistic forecasts (ECMWF EPS) are verified on actual observations (reanalysis and satellite).

The training data for InterpNet come from the operational deterministic day-ahead forecast model ECMWF IFS model interpolated to ERA5 grid ($0.25° \times 0.25°$) with an hourly resolution. The study area spans Europe, extending from 12° W to 32° E in longitude and from 33° N to 66° N in latitude. For training, every third hour is selected and the two hours in between are ignored as input but considered as the relevant outputs. Extraterrestrial irradiation values, used within the reference method and as inputs for InterpNet, are calculated using the `atlite` library. More specifically, these algorithms follow a deterministic procedure based on simple vector geometry [42,46,47]. Clear-sky irradiation is retrieved from the ECMWF ERA5 model [45]. For additional verification, the ensemble forecasts are verified using ERA5 reanalysis data [45] and SARAH-2.1 [48]. In addition to reanalysis data, satellite-derived irradiance maps are used due to their more accurate solar irradiance estimation [49–51]. Both data sets are used to investigate whether the performance differences of temporal interpolation techniques are still important considering different ground truths.

The training data covers the period of 2013–2015 and is validated on the year 2017. The test data covers the year 2016 whereas the probabilistic forecasts take the year 2015 and the first three months of 2016 as validation.

The code is implemented in `python` and the InterpNet is implemented in `pytorch` [34] trained on a Tesla V100 (16 GB) GPU. Data interpolation and preprocessing is implemented in `xarray` [52]. The plots are generated with `matplotlib` [53].

4.2. Forecast interpolation verification

To evaluate the skill to restore the omitted forecasts, the mean absolute error (MAE) is used, which is defined as

$$MAE(y, \hat{y}) = \frac{1}{N}\sum_{n=1}^{N}|y - \hat{y}| \tag{5}$$

To verify the ensemble forecasts, the continuous ranked probability score (CRPS) [54] is used. The CRPS measures the distance between the predicted and observed cumulative distribution function [55] and is the most common verification metric for probabilistic forecasts [1]. Mathematically, it is defined as

$$CRPS(F, x) = -\int_{-\infty}^{\infty}(F(y) - \mathbb{1}\{y \geq x\})^2 dy \tag{6}$$

with $\mathbb{1}$ heavy-side function. Technically, this corresponds to the integral of the better-known Brier score for binary probability forecasts [54,55], while we use the implementation based on the empirical distribution function implemented in the `properscoring` library. To relate the improvement of the forecasts to a reference forecast, skill scores (SS) are used [56], which relate the accuracy of the forecast accuracy A_f to the accuracy of a reference forecast A_r:

$$SS = 1 - \frac{A_f}{A_r} \tag{7}$$

Skill scores measure the performance gain from one forecast over another and how much of the potentially reachable skill improvement is provided by the new forecast. Therefore, a value of 0.5 means that 50% of the reachable skill score is obtained, a value of 0 means that there are no skill improvements and negative values represent worse forecasts [56]. In this study, we express skill scores in relation to the clear-sky linear interpolation as the strongest benchmark method. The skill scores are expressed for MAE and CRPS and averaged over the test period.

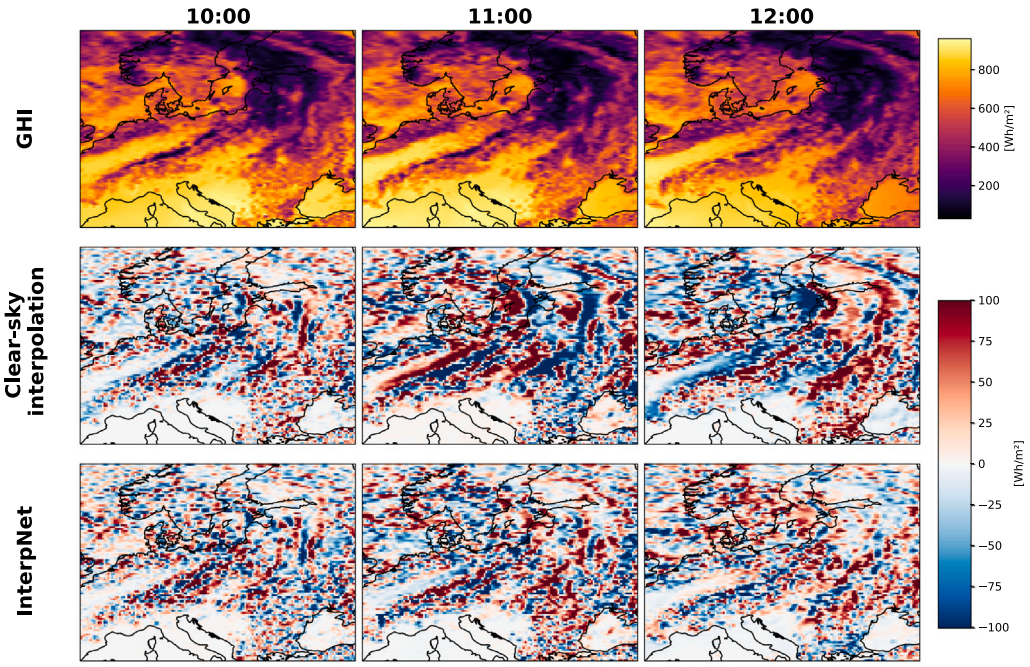

Fig. 5. InterpNet's performance against clear-sky interpolation. The first row indicates the actual forecasts to be restored, while the second and third row the error maps of the interpolation methods [Wh/m^2] (2017-06-12).

5. Results

5.1. Forecast restoration

5.1.1. Diurnal cycle bias

First, we visually investigate the results of the different methods, as shown in Fig. 4. Ignoring any normalization leads to a strong diurnal cycle bias as visible for the linear interpolation. The sign of this bias changes for the respective hour and aligns with the derived description in Section 3.2. Scaled linear interpolation manages to remove this bias as visible in the clearness and clear-sky interpolation. Yet, using clearness interpolation leads to a small bias particularly visible at 10:00 and 12:00, showing again both over-and underestimations. The clearsky-interpolation is able to completely filter this bias. Interestingly, InterpNet is also able to completely filter this bias despite relying on the clearness index. This shows that InterpNet can learn the diurnal cycle bias from the data even when only using the clearness index.

5.1.2. Non-linear modeling abilities

In addition to reducing the bias of the diurnal cycle, InterpNet shows different estimations at the position of the clouds, as shown in Fig. 5. When comparing clear-sky interpolations with those from InterpNet, there are notable differences in the cloud movement estimations in both sign and shape. This is, for instance, visible in the large cloud system, possibly due to a cold front in the upper left of the image that affects the northern parts of the United Kingdom. Although the clear-sky interpolation does not show a systematic bias, it is characterized by large errors because of the incorrect prediction of the movement of the clouds. In contrast, InterpNet leads to much smaller errors, indicating that it corrects not only the diurnal cycle bias but also improves the nonlinear modeling capabilities during complex weather situations. This is also noticeable in other regions in Fig. 5, such as in North-East Europe, where the clear-sky interpolation shows a large overestimation at 12:00, while InterpNet has much smaller errors in this region.

5.1.3. Performance under different solar altitude angles

The overall performance of InterpNet is evaluated by aggregating the performance throughout the test year, as provided in Table 2. Furthermore, the results are grouped by different solar altitude angles α. This separation is motivated by the circumstance that during sunset and sunrise (low solar altitude angles), solar irradiance estimates are often erroneous [8].

Intuitively, larger solar altitude angles lead to larger errors due to larger solar irradiation values. Normalization by clearness or clear-sky indices improves interpolation by more than 50%, while using the clear-sky index provides additional benefits. InterpNet beats clear-sky interpolation by around 32% aggregated over all solar altitude angles with a consistent decline of model improvements over clear-sky interpolation with lower solar altitude angles. The benefit of using InterpNet varies from 60% for very low angles (below 10 degrees) to around 13.5% for high solar elevations (above 60 degrees).

A plausible explanation for the reduced performance gains at higher solar altitude angles lies in the characteristics of the diurnal cycle. Around solar noon, solar radiation tends to be smoother and nearly flat under clear-sky conditions, resulting in smaller interpolation errors, even without normalization. This is reflected in the reduced benefit of clear-sky over clearness normalization in periods with high solar altitude angles. Larger performance improvements of the InterpNet for smaller solar altitude angles can be attributed to more frequent weather changes during the morning and afternoon, as well as model-specific biases in the clear-sky radiation during sunrise and sunset that the InterpNet can learn from historic data.

5.1.4. Performance under different cloud conditions

As a final evaluation of the deterministic forecasts, we evaluated performance under cloudy and cloudless conditions using the categorization described in Shi et al. [57]. As shown in Table 3, InterpNet provides reliable interpolations regardless of cloud conditions, with slightly greater improvements observed during cloudy conditions compared to those without clouds (approximately 34% versus 28%). This suggests that the non-linear modeling and incorporation of spatial information in InterpNet are beneficial for estimating cloud movement, outperforming linear interpolation methods that rely solely on

Table 2
Performance of forecast restoration (MAE) of respective methods overall and with different solar altitude angle α in 2017 in [W h m^{-2}]. The number in the brackets for the InterpNet represents the improvement over the clear-sky linear interpolation. The results are averaged over all grid points.

	$\alpha > 0°$ (all)	$0° < \alpha < 10°$	$10° < \alpha < 25°$	$25° < \alpha < 45°$	$45° < \alpha < 60°$	$\alpha > 60°$
Linear	57.3	37.2	57.7	67.4	63.7	54.9
Clearness	24.1	10.1	19.1	29.9	38.2	37.0
Clear-sky	19.7	8.1	16.7	24.4	30.8	25.1
InterpNet	13.3 (32.5%)	3.2 (60.5%)	9.0 (46.1%)	17.9 (26.6%)	25.6 (16.9%)	21.7 (13.5%)

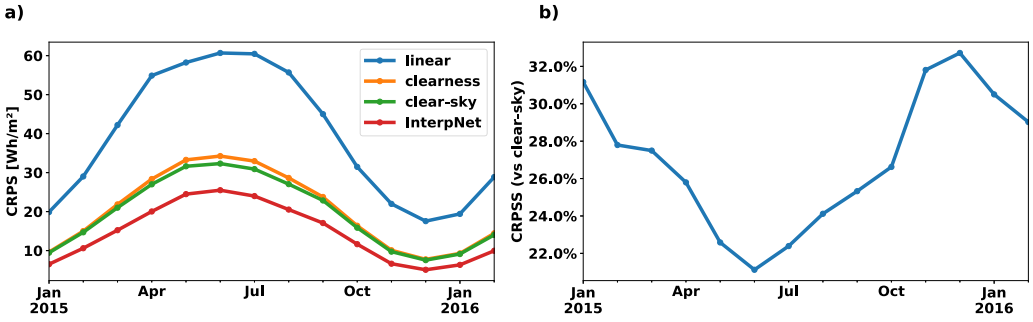

Fig. 6. Probabilistic benchmark: Annual course of Continuous Ranked Probability Score. (a) shows the performance of the different methods during the respective 14 months, (b) shows the performance improvements of the neural network over the clear-sky interpolation. The results are averaged over all grid points.

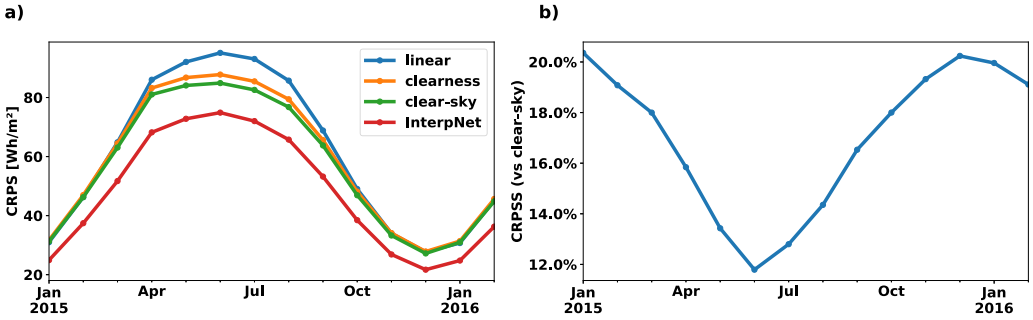

Fig. 7. Identical to Fig. 6 but for the SARAH 2.1 dataset.

Table 3
Performance (in percentage) in forecast restoration (MAE) of respective methods in cloudy and cloudless conditions in 2017 in [W h m^{-2}]. The results are averaged over all grid points.

	Cloudless	Cloudy
Linear	58.0	57.2
Clearness	32.4	22.5
Clear-sky	30.4	17.6
InterpNet	21.9 (28.0%)	11.6 (34.1%)

single-point estimates and ignore information from surrounding grid points.

5.2. Probabilistic forecast performance

To evaluate the expected improvements of using InterpNet for observations and for ensemble forecasting, we also evaluated the performance based on reanalysis data (ERA5) and satellite-derived irradiation data (SARAH 2.1). The monthly CRPS for the ERA5 data is shown in Fig. 6. Throughout the year, linear interpolation shows large interpolation errors, which can be reduced by more than 50% by using clearness and clear-sky interpolations. In this case, the difference between clearness and clear sky interpolation becomes minor but significant, as evaluated by stationary block bootstrapping with a mean monthly CRPS difference of 0.88 (95% CI 0.39 – 1.40; 10 000 resamples). As this value remains positive within the confidence interval, clear-sky interpolation is statistically better than clearness interpolation. Similarly to the performance in forecast restoration, InterpNet's predictions constantly outperform the other benchmark methods. The improvements in clear sky interpolation are between 20% and 30% with the highest improvements during winter and smaller improvements during summer (more than 22%). This can be explained by the circumstance that during the winter months more hours are characterized by lower solar altitude angles than during the summer months and the InterpNet shows the largest improvements during low solar altitude angles.

As ERA5 is based on a dynamical model known to lead to insufficient solar radiation estimations, it raises the question whether the skill improvements are also observable for datasets closer to actual observations. For this purpose, we use satellite-based irradiation estimates in the following (Sarah-2.1) because they are known to provide a better estimate of the actual irradiation situation (Fig. 7). As expected, the overall error increases, yet the distinct differences between the interpolation methods are noticeable showing CRPSS between 12 and 20% which is around 10% less than using ERA5 as observations, but still considered to be large. Similarly to ERA5, the differences between clarity and clear-sky interpolations are minor, yet significant, as also evaluated by stationary block bootstrapping as for ERA5 with mean monthly differences of 0.88 (95% CI 0.84 – 2.25; 10 000 resamples) that are larger than ERA5, yet remain minor.

6. Discussion

In this study, we focused on linear interpolation methods as benchmark methods due to their prominent usage. These methods are widely used, and linear clear-sky interpolation is commonly used for solar irradiance interpolation [16,17,58,59]. However, this raises the question whether more sophisticated models, such as cubic or spline regressions, could be a stronger benchmarking method. During the experiments conducted in this study, we evaluated cubic and spline regressions on both raw and clear-sky normalized irradiation values, which did not show promise. Although they could improve simple linear interpolation, they were still worse than using linear clearness or clear-sky interpolations. This is also in agreement with Girodo [60], who claims that fitting polynomials can lead to strong overestimation during noon hours. As these methods are rare and did not show promise, they were left out of the analyses of this study.

With respect to InterpNet's performance, further improvements can be expected by integrating the clear-sky index instead of the clearness index into the model architecture. We focused on using the clearness index, as it is NWP model independent and can be rapidly calculated using deterministic algorithms. Furthermore, given that the improvements of the clear-sky interpolation were minor compared to the clearness interpolation for the ensemble forecast comparison, the expected benefit is arguably too small to justify the efforts to use model-dependent, computationally heavy clear-sky index calculations. The fact that neural networks with the clearness index can outperform the clear-sky index for solar forecasting has also been shown by Lauret et al. [61], however, they also show that the improvement of using the clear-sky index over the clearness index can be small and varies subject to the site specifics.

Furthermore, this study focuses on the European domain, raising the question of whether the model is transferable to other regions. In Ruan et al. [62], it was shown that a U-Net-based architecture can be reliably used to transfer a spatio-temporal solar irradiance forecasting model to an unseen region. Therefore, it is likely that the InterpNet architecture is able to generalize to an unseen region.

7. Summary

This study proposes InterpNet, a method to derive missing time steps from NWP irradiation forecasts. Compared to other commonly used interpolation methods, such as linear or scaled interpolation, InterpNet consistently shows much better performance for both deterministic and ensemble forecasts at different solar altitude angles and under different cloud conditions. The only auxiliary input required is extraterrestrial irradiation, a quantity that can easily be calculated with deterministic algorithms. This makes the proposed method easy to use and highly scalable for operational usage. Future research could explore other input variables to improve the estimation of the spatio-temporal dynamics of the clouds to better approximate the physical processes such as advection and diffusion. Furthermore, more research is needed to determine whether the results of this study generalize to arbitrary time steps and not only to hourly time steps as in this study.

CRediT authorship contribution statement

Matthias Zech: Writing – review & editing, Writing – original draft, Visualization, Validation, Supervision, Software, Resources, Project administration, Methodology, Investigation, Funding acquisition, Formal analysis, Data curation. **Annette Hammer:** Writing – review & editing, Writing – original draft, Supervision, Methodology, Conceptualization. **Lueder von Bremen:** Writing – review & editing, Project administration, Funding acquisition, Data curation.

Declaration of competing interest

The authors declare that they have no known competing financial interests or personal relationships that could have appeared to influence the work reported in this paper.

Acknowledgments

The presented work has been carried out within the national research project "SOLREV" (FKZ 03EE1010E) funded by the Federal Ministry for Economic Affairs and Climate Action, Germany (BMWK) on the basis of a decision by the German Bundestag. M. Zech has been supported by the German Federal Environmental Foundation within the PhD scholarship (grant no. 20020/667-33/2). The authors thank the project members of the SOLREV project and the energy meteorology group for interesting discussions that have improved this paper. Furthermore, the authors would like to thank the German Aerospace Center for providing computing facilities for the computational experiments conducted in this study.

Data availability

The reanalysis data (ERA5) and the satellite data (SARAH 2.1) used for validation are retrieved through the `atlite` library. Further information about how to download and pre-process these data can be found in the respective documentation. The used deterministic and EPS NWP forecasts are available on request.

References

[1] P. Lauret, M. David, P. Pinson, Verification of solar irradiance probabilistic forecasts, Sol. Energy 194 (September) (2019) 254–271, http://dx.doi.org/10.1016/j.solener.2019.10.041.

[2] A.J. Conejo, M. Carrión, J.M. Morales, Decision Making Under Uncertainty in Electricity Markets, first ed., Springer, New York, 2010, http://dx.doi.org/10.1007/978-1-4419-7421-1.

[3] J.M. Morales, M. Zugno, S. Pineda, P. Pinson, Electricity market clearing with improved scheduling of stochastic production, European J. Oper. Res. 235 (3) (2014) 765–774, http://dx.doi.org/10.1016/j.ejor.2013.11.013.

[4] M. Lubin, C.G. Petra, M. Anitescu, V. Zavala, Scalable stochastic optimization of complex energy systems, in: Proceedings of 2011 SC - International Conference for High Performance Computing, Networking, Storage and Analysis, 2011, http://dx.doi.org/10.1145/2063384.2063470.

[5] E. Kraft, M. Russo, D. Keles, V. Bertsch, Stochastic optimization of trading strategies in sequential electricity markets, European J. Oper. Res. (xxxx) (2022) http://dx.doi.org/10.1016/j.ejor.2022.10.040.

[6] R. Perez, S. Kivalov, J. Schlemmer, K. Hemker, Validation of short and medium term operational solar radiation forecasts in the US, SOLAR 2009, in: 38th ASES National Solar Conference 2009, vol. 5, no. 2010, 2009, pp. 3079–3084.

[7] M. Diagne, M. David, P. Lauret, J. Boland, N. Schmutz, Review of solar irradiance forecasting methods and a proposition for small-scale insular grids, Renew. Sustain. Energy Rev. 27 (2013) 65–76, http://dx.doi.org/10.1016/j.rser.2013.06.042.

[8] A. Betti, P. Blanc, M. David, Y.-M. Saint-Drenan, A. Driesse, J. Freeman, R. Fritz, C. Gueymard, A. Habte, R. Höller, J. Huang, A. Kazantzidis, J. Kleissl, C. Köhler, T. Landelius, V. Lara-Fanego, E. Lorenz, P. Lauret, L. Martin, M. Mehos, R. Meyer, D. Myers, K.P. Nielsen, R. Perez, C.F. Peruchena, J. Polo, D. Renné, L. Ramírez, J. Remund, J.A. Ruiz-Arias, M. Sengupta, M. Silva, D. Spieldenner, T. Stoffel, M. Suri, S. Wilbert, S. Wilcox, F. Vignola, P. Wang, Y. Xie, L.F. Zarzalejo, Best Practices Handbook for the Collection and Use of Solar Resource Data for Solar Energy Applications: Third Edition Task 16 Solar Resource for High Penetration and Large Scale Applications, IEA PVPS, 2021, p. 331, URL: www.iea-pvps.org.

[9] P. Bauer, A. Thorpe, G. Brunet, The quiet revolution of numerical weather prediction, Nature 525 (7567) (2015) 47–55, http://dx.doi.org/10.1038/nature14956.

[10] R. Buizza, P.L. Houtekamer, Z. Toth, G. Pellerin, M. Wei, Y. Zhu, A Comparison of the ECMWF, MSC, and NCEP Global Ensemble Prediction Systems, Technical Report, 2005.

[11] P. Gronquist, C. Yao, T. Ben-Nun, N. Dryden, P. Dueben, S. Li, T. Hoefler, Deep learning for post-processing ensemble weather forecasts, Philos. Trans. R. Soc. A: Math., Phys. Eng. Sci. 379 (2194) (2021) http://dx.doi.org/10.1098/rsta.2020.0092.

[12] M. Leutbecher, T.N. Palmer, Ensemble forecasting, J. Comput. Phys. 227 (7) (2008) 3515–3539, http://dx.doi.org/10.1016/j.jcp.2007.02.014.

[13] J. Thorey, V. Mallet, C. Chaussin, L. Descamps, P. Blanc, Ensemble forecast of solar radiation using TIGGE weather forecasts and HelioClim database, Sol. Energy 120 (2015) 232–243, http://dx.doi.org/10.1016/j.solener.2015.06.049.

[14] S. Sperati, S. Alessandrini, L. Delle Monache, An application of the ECMWF Ensemble Prediction System for short-term solar power forecasting 1 2, Technical Report, 2016, URL: http://www.elsevier.com/open-access/userlicense/1.0/.

[15] E. Lorenz, J. Hurka, D. Heinemann, H.G. Beyer, Irradiance forecasting for the power prediction of grid-connected photovoltaic systems, IEEE J. Sel. Top. Appl. Earth Obs. Remote. Sens. 2 (1) (2009) 2–10, http://dx.doi.org/10.1109/JSTARS.2009.2020300.

[16] E. Lorenz, J. Remund, S.C. Müller, W. Traunmüller, G. Steinmaurer, D. Pozo, J.A. Ruiz-Arias, V.L. Fanego, L. Ramirez, M.G. Romeo, C. Kurz, L.M. Pomares, C. Guerrero, Benchmarking of different approaches to forecast solar irradiance, Eur. Photovolt. Sol. Energy Conf. (2009) 4199–4208, http://dx.doi.org/10.4229/24thEUPVSEC2009-5BV.2.50.

[17] M. Sengupta, Y. Xie, A. Lopez, A. Habte, G. Maclaurin, J. Shelby, The national solar radiation data base (NSRDB), Renew. Sustain. Energy Rev. 89 (January 2018) (2018) 51–60, http://dx.doi.org/10.1016/j.rser.2018.03.003.

[18] A.H. Nielsen, A. Iosifidis, H. Karstoft, IrradianceNet: Spatiotemporal deep learning model for satellite-derived solar irradiance short-term forecasting, Sol. Energy 228 (2021) 659–669, http://dx.doi.org/10.1016/j.solener.2021.09.073.

[19] A. Carpentieri, D. Folini, J. Leinonen, A. Meyer, Extending intraday solar forecast horizons with deep generative models, Appl. Energy 377 (2025) http://dx.doi.org/10.1016/j.apenergy.2024.124186.

[20] P. Gentine, M. Pritchard, S. Rasp, G. Reinaudi, G. Yacalis, Could machine learning break the convection parameterization deadlock? Geophys. Res. Lett. 45 (11) (2018) 5742–5751, http://dx.doi.org/10.1029/2018GL078202.

[21] D.J. Gagne, H.M. Christensen, A.C. Subramanian, A.H. Monahan, Machine learning for stochastic parameterization: Generative adversarial networks in the Lorenz '96 model, J. Adv. Model. Earth Syst. 12 (3) (2020) http://dx.doi.org/10.1029/2019MS001896.

[22] S. Rasp, M.S. Pritchard, P. Gentine, Deep learning to represent subgrid processes in climate models, Proc. Natl. Acad. Sci. USA 115 (39) (2018) 9684–9689, http://dx.doi.org/10.1073/pnas.1810286115, URL: https://gitlab.com/mspritch/spcam3.0-neural-net/tree/nn.

[23] A. Chattopadhyay, A. Subel, P. Hassanzadeh, Data-driven super-parameterization using deep learning: Experimentation with multiscale lorenz 96 systems and transfer learning, J. Adv. Model. Earth Syst. 12 (11) (2020) http://dx.doi.org/10.1029/2020MS002084.

[24] J.W. Messner, G.J. Mayr, A. Zeileis, Nonhomogeneous boosting for predictor selection in ensemble postprocessing, Mon. Weather Rev. 145 (1) (2017) 137–147, http://dx.doi.org/10.1175/MWR-D-16-0088.1.

[25] B. Schulz, S. Lerch, Machine learning methods for postprocessing ensemble forecasts of wind gusts: A systematic comparison, Mon. Weather Rev. 150 (1) (2022) 235–237, http://dx.doi.org/10.1175/MWR-D-21-0150.1.

[26] S. Rasp, S. Lerch, Neural networks for postprocessing ensemble weather forecasts, Mon. Weather Rev. 146 (11) (2018) 3885–3900, http://dx.doi.org/10.1175/MWR-D-18-0187.1.

[27] S. Rasp, N. Thuerey, Data-driven medium-range weather prediction with a resnet pretrained on climate simulations: A new model for WeatherBench, J. Adv. Model. Earth Syst. 13 (2) (2021) http://dx.doi.org/10.1029/2020MS002405.

[28] R. Lam, A. Sanchez-Gonzalez, M. Willson, P. Wirnsberger, M. Fortunato, F. Alet, S. Ravuri, T. Ewalds, Z. Eaton-Rosen, W. Hu, A. Merose, S. Hoyer, G. Holland, O. Vinyals, J. Stott, A. Pritzel, S. Mohamed, P. Battaglia, Learning skillful medium-range global weather forecasting, Technical Report 6677, in: Science, vol. 382, 2023, pp. 1416–1422, http://dx.doi.org/10.1126/science.adi2336.

[29] I. Price, A. Sanchez-Gonzalez, F. Alet, T.R. Andersson, A. El-Kadi, D. Masters, T. Ewalds, J. Stott, S. Mohamed, P. Battaglia, R. Lam, M. Willson, Probabilistic weather forecasting with machine learning, Nature (2024) http://dx.doi.org/10.1038/s41586-024-08252-9.

[30] S. Lang, M. Alexe, M. Chantry, J. Dramsch, F. Pinault, B. Raoult, M.C.A. Clare, C. Lessig, M. Maier-Gerber, L. Magnusson, Z.B. Bouallègue, A.P. Nemesio, P.D. Dueben, A. Brown, F. Pappenberger, F. Rabier, AIFS – ECMWF's data-driven forecasting system, 2024, URL: http://arxiv.org/abs/2406.01465.

[31] S. Rasp, S. Hoyer, A. Merose, I. Langmore, P. Battaglia, T. Russell, A. Sanchez-Gonzalez, V. Yang, R. Carver, S. Agrawal, M. Chantry, Z. Ben Bouallegue, P. Dueben, C. Bromberg, J. Sisk, L. Barrington, A. Bell, F. Sha, WeatherBench 2: A benchmark for the next generation of data-driven global weather models, J. Adv. Model. Earth Syst. 16 (6) (2024) http://dx.doi.org/10.1029/2023MS004019.

[32] R.W. Riddaway, Meteorological Training Course Lecture Series Numerical methods Revised March 2001, Technical Report, 2001.

[33] O. Ronneberger, P. Fischer, T. Brox, U-net: Convolutional networks for biomedical image segmentation, in: Lecture Notes in Computer Science (Including Subseries Lecture Notes in Artificial Intelligence and Lecture Notes in Bioinformatics), vol. 9351, 2015, pp. 234–241, http://dx.doi.org/10.1007/978-3-319-24574-4{_}28.

[34] A. Paszke, S. Gross, F. Massa, A. Lerer, J. Bradbury, G. Chanan, T. Killeen, Z. Lin, N. Gimelshein, L. Antiga, A. Desmaison, A. Köpf, E. Yang, Z. DeVito, M. Raison, A. Tejani, S. Chilamkurthy, B. Steiner, L. Fang, J. Bai, S. Chintala, Pytorch: An imperative style, high-performance deep learning library, Adv. Neural Inf. Process. Syst. 32 (2019).

[35] X. Hou, B. Wang, W. Hu, L. Yin, H. Wu, SolarNet: A deep learning framework to map solar power plants in China from satellite imagery, in: ICLR 2020 Workshop on Tackling Climate Change with Machine Learning, 2020, URL: http://arxiv.org/abs/1912.03685.

[36] M. Zech, H.P. Tetens, J. Ranalli, Toward global rooftop PV detection with deep active learning, Adv. Appl. Energy 16 (August) (2024) 100191, http://dx.doi.org/10.1016/j.adapen.2024.100191.

[37] I. Goodfellow, Y. Bengio, A. Courville, Deep Learning, vol. 521, no. 7553, MIT Press, 2017, p. 785, http://dx.doi.org/10.1016/B978-0-12-391420-0.09987-X.

[38] K. He, X. Zhang, S. Ren, J. Sun, Deep residual learning for image recognition, in: Proceedings of the IEEE Conference on Computer Vision and Pattern Recognition, 2016, pp. 770–778.

[39] S. Marcel, Y. Rodriguez, Torchvision the machine-vision package of torch, in: MM'10 - Proceedings of the ACM Multimedia 2010 International Conference, Association for Computing Machinery, 2010, pp. 1485–1488, http://dx.doi.org/10.1145/1873951.1874254.

[40] D.P. Kingma, J.L. Ba, Adam: A method for stochastic optimization, 3rd Int. Conf. Learn. Represent. ICLR 2015 - Conf. Track Proc. (2015) URL: http://arxiv.org/abs/1412.6980.

[41] L.N. Smith, N. Topin, Super-convergence: very fast training of neural networks using large learning rates, Artif. Intell. Mach. Learn. Multi-Domain Oper. Appl. 11006 (2019) 369–386, http://dx.doi.org/10.1117/12.2520589.

[42] S.A. Kalogirou, Solar energy engineering: Processes and systems: Second edition, Sol. Energy Eng.: Process. Syst.: Second. Ed. (2014) 1–819, http://dx.doi.org/10.1016/C2011-0-07038-2.

[43] J. Antonanzas, N. Osorio, R. Escobar, R. Urraca, F.J. Martinez-de Pison, F. Antonanzas-Torres, Review of photovoltaic power forecasting, in: Solar Energy, vol. 136, Elsevier Ltd, 2016, pp. 78–111, http://dx.doi.org/10.1016/j.solener.2016.06.069.

[44] F. Antonanzas-Torres, R. Urraca, J. Polo, O. Perpiñán-Lamigueiro, R. Escobar, Clear sky solar irradiance models: A review of seventy models, Renew. Sustain. Energy Rev. 107 (February) (2019) 374–387, http://dx.doi.org/10.1016/j.rser.2019.02.032.

[45] H. Hersbach, B. Bell, P. Berrisford, S. Hirahara, A. Horányi, J. Muñoz-Sabater, J. Nicolas, C. Peubey, R. Radu, D. Schepers, A. Simmons, C. Soci, S. Abdalla, X. Abellan, G. Balsamo, P. Bechtold, G. Biavati, J. Bidlot, M. Bonavita, G. De Chiara, P. Dahlgren, D. Dee, M. Diamantakis, R. Dragani, J. Flemming, R. Forbes, M. Fuentes, A. Geer, L. Haimberger, S. Healy, R.J. Hogan, E. Hólm, M. Janisková, S. Keeley, P. Laloyaux, P. Lopez, C. Lupu, G. Radnoti, P. de Rosnay, I. Rozum, F. Vamborg, S. Villaume, J.N. Thépaut, The ERA5 global reanalysis, Q. J. R. Meteorol. Soc. 146 (730) (2020) 1999–2049, http://dx.doi.org/10.1002/qj.3803.

[46] A.B. Sproul, Derivation of the solar geometric relationships using vector analysis, Renew. Energy 32 (7) (2007) 1187–1205, http://dx.doi.org/10.1016/j.renene.2006.05.001.

[47] D.T. Reindl, W.A. Beckman, J.A. Duffie, Diffuse fraction correlations, Sol. Energy 45 (1) (1990) 1–7, http://dx.doi.org/10.1016/0038-092X(90)90060-P.

[48] U. Pfeifroth, S. Kothe, J. Trentmann, R. Hollmann, P. Fuchs, J. Kaise, M. Werscheck, Surface radiation data set - heliosat (SARAH) - edition 2.1, 2019, http://dx.doi.org/10.5676/EUM{_}SAF{_}CM/SARAH/V002{_}01.

[49] C.W. Frank, The Potential of High Resolution Regional Reanalyses COSMO-REA for Renewable Energy Application (Ph.D. thesis), Universität zu Köln, 2020, p. 156, URL: http://kups.ub.uni-koeln.de/id/eprint/10857.

[50] S. Pfenninger, I. Staffell, Long-term patterns of European PV output using 30 years of validated hourly reanalysis and satellite data, Energy 114 (2016) 1251–1265, http://dx.doi.org/10.1016/j.energy.2016.08.060.

[51] R. Urraca, T. Huld, A. Gracia-Amillo, F.J. Martinez-de Pison, F. Kaspar, A. Sanz-Garcia, Evaluation of global horizontal irradiance estimates from ERA5 and COSMO-REA6 reanalyses using ground and satellite-based data, Sol. Energy 164 (2018) 339–354, http://dx.doi.org/10.1016/j.solener.2018.02.059.

[52] S. Hoyer, J. Hamman, Xarray: N-D labeled arrays and datasets in python, J. Open Res. Softw. 5 (1) (2017) 10, http://dx.doi.org/10.5334/jors.148.

[53] J.D. Hunter, Matplotlib: A 2D graphics environment, Comput. Sci. Eng. 9 (3) (2007) 90–95.

[54] T. Gneiting, A.E. Raftery, Strictly proper scoring rules, prediction, and estimation, J. Amer. Statist. Assoc. 102 (477) (2007) 359–378, http://dx.doi.org/10.1198/016214506000001437.

[55] H. Hersbach, Decomposition of the continuous ranked probability score for ensemble prediction systems, Weather. Forecast. 15 (5) (2000) 559–570, http://dx.doi.org/10.1175/1520-0434(2000)015<0559:DOTCRP>2.0.CO;2.

[56] E. Wheatcroft, Interpreting the skill score form of forecast performance metrics, Int. J. Forecast. 35 (2) (2019) 573–579, http://dx.doi.org/10.1016/j.ijforecast.2018.11.010.

[57] H. Shi, D. Yang, W. Wang, D. Fu, L. Gao, J. Zhang, B. Hu, Y. Shan, Y. Zhang, Y. Bian, H. Chen, X. Xia, First estimation of high-resolution solar photovoltaic resource maps over China with Fengyun-4A satellite and machine learning, Renew. Sustain. Energy Rev. 184 (June) (2023) http://dx.doi.org/10.1016/j.rser.2023.113549.

[58] P. Mathiesen, J. Kleissl, Evaluation of numerical weather prediction for intra-day solar forecasting in the continental United States, Sol. Energy 85 (5) (2011) 967–977, http://dx.doi.org/10.1016/j.solener.2011.02.013.

[59] R.A. Verzijlbergh, P.W. Heijnen, S.R. de Roode, A. Los, H.J. Jonker, Improved model output statistics of numerical weather prediction based irradiance forecasts for solar power applications, Sol. Energy 118 (2015) 634–645, http://dx.doi.org/10.1016/j.solener.2015.06.005.

[60] M. Girodo, Solarstrahlungsvorhersage auf der Basis numerischer Wettermodelle (Ph.D. thesis), University of Oldenburg, 2006.

[61] P. Lauret, R. Alonso-Suárez, J. Le Gal La Salle, M. David, Solar forecasts based on the clear sky index or the clearness index: Which is better? Solar 2 (4) (2022) 432–444, http://dx.doi.org/10.3390/solar2040026.

[62] Z. Ruan, W. Sun, Y. Yuan, H. Tan, Accurately forecasting solar radiation distribution at both spatial and temporal dimensions simultaneously with fully-convolutional deep neural network model, Renew. Sustain. Energy Rev. 184 (June) (2023) 113528, http://dx.doi.org/10.1016/j.rser.2023.113528.